Reduced methane seepage from Arctic sediments during cold bottom water conditions

Bénédicte Ferré[1*], Pär G. Jansson[1], Manuel Moser[1], Pavel Serov[1], Alexey Portnov[1,2], Carolyn Graves[3,4], Giuliana Panieri[1], Friederike Gründger[1], Christian Berndt[5], Moritz F. Lehmann[6], Helge Niemann[1,6,7,8]

* Correspondence to: benedicte.ferre@uit.no

[1]CAGE-Centre for Arctic Gas Hydrate, Environment and Climate, Department of Geosciences, The Arctic University of Norway, 9037 Tromsø, Norway.

[2]School of Earth Sciences, The Ohio State University, Columbus, Ohio 43210, USA.

[3]Baltic Sea Research Institute, IOW, 18119 Rostock-Warnemuende, Germany.

[4]Currently at Centre for Environment, Fisheries and Aquaculture Science (Cefas), Lowestoft, Suffolk, NR33 0HT, UK.

[5]GEOMAR Helmholtz Centre for Ocean Research Kiel, 24148 Kiel, Germany.

[6]Department of Environmental Science, University of Basel, 4056 Basel, Switzerland.

[7]NIOZ Royal Netherlands Institute for Sea Research, Department of Marine Microbiology & Biogeochemistry, and Utrecht University, 1797 SZ 't Horntje, the Netherlands

[8]Department of Earth Sciences, Faculty of Geosciences, Utrecht University, 3508 TC Utrecht, the Netherlands

Large amounts of methane are trapped within gas hydrate in sub-seabed sediments in the Arctic Ocean, and bottom-water warming may induce the release of methane from

the seafloor. Yet, the effect of seasonal temperature variations on methane seepage activity remains unknown, as surveys in Arctic seas are mainly conducted in summer. Here, we compare the activity of cold seeps along the gas hydrate stability limit offshore Svalbard during cold (May 2016) and warm (August 2012) seasons. Hydro-acoustic surveys revealed a substantially decreased seepage activity during cold bottom-water conditions, corresponding to a 43 % reduction of total cold seeps and methane release rates compared to warmer conditions. We demonstrate that cold seeps apparently hibernate during cold seasons, when more methane gas becomes trapped in the sub-seabed sediments. Such a greenhouse gas capacitor increases the potential for methane release during summer months. Seasonal bottom-water temperature variations are common on the Arctic continental shelves. We infer that methane-seep hibernation is a widespread phenomenon that is underappreciated in global methane budgets, leading to overestimates in current calculations.

Methane (CH_4) is a particularly important trace gas, as its atmospheric concentration has almost tripled since the beginning of industrialisation[1]. With an equivalent warming potential that is 32 times higher than that of carbon dioxide[2], it contributes 16 % to the global greenhouse effect[1], and has a lifetime of ~12 years in the atmosphere[3]. Natural CH_4 emissions have diverse origins and vary in space and time[4], increasing the uncertainty of the contribution of natural sources to the bulk atmospheric CH_4 budget. Arctic Ocean sediments host enormous CH_4 reservoirs, in the form of free gas, dissolved in pore water, or trapped in permafrost and gas hydrates[5-9]. Gas hydrates are stable at low temperature and high pressure[10], conditions typically found at ≳400 m water depth. They can dissociate if the ambient temperature rises[11], and there is evidence for large-scale CH_4 eruptions due to warming of hydrate-bearing sediments in the geological past[12,13].

Based on median climate response scenarios, global mean surface temperatures are predicted to increase from 3.7 to 4.8 °C compared to pre-industrial levels by the end of the 21st century[1], and even more drastically in the Arctic with an estimated increase of 3 to 13 °C (ref. 14). The anticipated increase of surface heat will propagate through the water column[15] and eventually into sediments[11,16,17]. There, it can lead to gas hydrate dissociation and the release of free and dissolved CH_4 to the water column and potentially to the atmosphere, further contributing to global warming. However, the contribution of seafloor CH_4 outgassing to climate change is uncertain, and ~90% of the CH_4 rising through the seabed is consumed by microbial oxidation near the sediment-water interface and in the water column before it can reach the atmosphere[18]. The efficiency of this biological filter is modulated by several factors, including ocean currents[19], nutrient availability[20], redox dynamics[18], methane concentration and temperature[21].

The Norwegian Arctic is prone to large seasonal water temperature variability[22]. While the global warming effect on increasing water temperature has been studied intensively (e.g. 23), the impact of seasonal temperature fluctuations on CH_4 emissions remains largely unknown[24-26]. The ongoing CH_4 emission at the termination of the gas hydrate stability zone (GHSZ) (ref. 27-30) off western Svalbard has been related to gas hydrate dissociation due to anthropogenic water-column warming[29]. However, seepage in this area has been active for >3000 years[26], and hydrates started dissociating ~8000 years ago when rapid glacial isostatic uplift overcame the sea level rise[31]. Today, ongoing CH_4 seepage likely originates primarily from free gas migrating along sedimentary layers or tectonic faults[32,33]. Seasonal variation of bottom-water temperatures lead to an annual deepening of the shallow boundary of the GHSZ from ~360 m (April-June, coldest bottom water temperatures) to >410 m depth (November-March, warmest bottom water temperatures)[26]. Previous hydro-acoustic surveys of CH_4 seepage were conducted in summer[30,32,34,35], as sea-going expeditions in polar regions depend on favourable

71 weather and sea ice conditions. The potential effect of seasonal temperature variation on
72 seepage activity remained unconstrained.

73 To investigate Arctic gas seepage during cold seasons, we conducted a research expedition
74 with the R/V *Helmer Hanssen* near the shelf break west of Svalbard from May 1st to 9th, 2016,
75 i.e. when coldest bottom-water temperatures of the year can be expected[26]. We explored
76 seepage activity along the outcrop of the GHSZ.

77 **Gas flare density and methane release from the seafloor**

78 The total number of gas flares (hydro-acoustic signatures of gas ebullition) was substantially
79 lower in May 2016 (196 flares) than in August 2012 (344 flares) (Fig. 1, Table 1). During
80 both surveys, most flares were observed between 360 and 400 meters water depth (Fig. 2).
81 Yet, during cold water conditions, there was a greater reduction in flare density at shallower
82 water depth (i.e., ~3 fold at 360-380 m water depth compared to ~1.5 fold at 400-380 m; Figs.
83 1 and 2), consistent with a net shallowing of the GHSZ limit[26].

84 To compare overall CH_4 fluxes from the sediment into the water column during cold and
85 warm bottom-water conditions, we applied a corrected parametrisation approach adopted from
86 Sahling et al.[30] (see Methods): i.e., assuming that each hydro-acoustically detected flare
87 cluster comprises six individual bubble streams with a CH_4 flow rate of ~37.1 mmol min^{-1},
88 and bottom water bubbles consist of pure CH_4. With these assumptions, methane release rates
89 from the seabed were 43 % lower during cold compared to warm season (Table 1). Given that
90 we applied the same flux quantification method for both surveys, our results provide robust
91 evidence that the flare activity is strongly reduced during wintertime when the bottom-water
92 temperatures are substantially lower than in summer.

93 The quantification approach of Sahling et al.[30] was based on a limited number of visual
94 seafloor observations and bubble catcher measurements. We applied a second, independent
95 approach to more accurately quantify CH_4 fluxes. We re-processed our high-resolution
96 echosounder data from May 2016 with the FlareHunter software package, which allows the
97 determination of CH_4 flow rates of individual flares and the integration of free gas emission
98 over large areas[34]. This method revealed highly variable flow rates between flare clusters,
99 ranging from 2 to 1,900 ml min^{-1} (Extended Data Figs. 1 and 2). The differential flow rates, in
100 turn, amount to a total CH_4 release rate of ~33 mol CH_4 min^{-1} from the seafloor in the study
101 area during cold conditions (Table 1). This is 25 % lower than the estimates based on the
102 corrected parametrisation of Sahling et al.[30]. Accounting for this apparent methodological
103 bias, we expect that the summertime CH_4 release rates are also 25 % lower compared to flux
104 estimates based on the Sahling et al.[30] parametrisation, i.e. 58 rather than 77 mol CH_4 min^{-1}.

105 **Water column biogeochemistry**

106 Bottom-water temperature in May 2016 was lower (1.7 °C) and salinity slightly higher
107 (between 34.9 and 35.1 PSU, Extended Data Fig. 3, Supplementary Table 2) than in August
108 2012 (3.5 °C; 33.7-35.2 PSU) (ref. 19) (Table 1). More importantly, the highest bottom-water
109 CH_4 concentrations measured during two transect samplings in May 2016 ranged between 20-
110 111 nmol l^{-1} (Extended Data Fig. 3), while they exceeded 400 nmol l^{-1} in August 2012 (ref.
111 19). The average water column CH_4 concentration in May 2016 was <5 nmol l^{-1}, which is
112 ~80% lower than in August 2012 (~25 nmol l^{-1}, Table 1).

113 Surface water CH_4 concentrations were less than 2 nmol l^{-1} (atmospheric equilibrium
114 concentration ~4 nM), rendering this region a negligible CH_4 source to the atmosphere during
115 cold season (see also Supplementary Information S.I.3). In contrast, during August 2012,

supersaturation in surface waters was significantly higher, with an average CH_4 concentration of 9 nmol l^{-1} (ref. 19).

Implications for seasonal variations of seafloor methane release

While our understanding of the potential controls on marine CH_4 emissions from the water column to the atmosphere has improved over the last decade[4,19,36], controls on temporal variability of CH_4 release from the seafloor to the ocean water column are largely unconstrained. The activity of some types of cold seeps, such as mud volcanoes and pockmarks, fluctuates on millennial time scales and may be erratic on shorter time scales of minutes to days[37]. Tides[38,39], natural seismicity[40] and long-term temperature rise[26,29] have been found to trigger abrupt CH_4 release from sediments. In general, the prediction of such episodic CH_4 release is difficult, complicating quantitative regional or global estimates of marine CH_4 emissions. Our data demonstrate for the first time that cold seep activity at the upper boundary of the GHSZ is modulated by seasonal temperature fluctuations. Bottom-water temperatures at this depth vary between ~1 °C in April-June and 5 °C in November-March[26]. Such bottom-water warming will affect the equilibrium between pressure and temperature causing a decrease in the pore pressure and the deepening of the shallow boundary of the GHSZ[26,29,41]. Downslope migration of the GHSZ proceeds to a water depth where the hydrostatic pressure is high enough to balance the temperature rise. In our study area, the GHSZ shifts from~360 m (April-June) to >410 m water depth (November-March), exposing an extensive seafloor area to non-hydrate thermobaric conditions. This seasonal shift of the GHSZ limit thus suggests the formation of gas hydrates in the upper sediments during the cold season. This is fuelled by rising CH_4, which will, at least partly, freeze as gas hydrate in shallow sediments below the seasonal termination of the GHSZ[42] (Fig. 3). Indeed, shallow bright spots with reversed polarity in the seismic data across the study area suggest free gas accumulations

immediately below the seafloor[41], and there is likely enough methane migrating upslope to form hydrate[43]. Hydrate can then form rapidly[44], and we therefore argue that the low temperatures consolidate small hydrate patches in the uppermost sediments building up a gas hydrate capacitor[45] that becomes depleted when the hydrates dissociate during summertime[26]. Indeed, temperature rise is expected to force CH_4 seep locations to migrate up-slope with the deepening GHSZ[26]. We observed a clear reduction of the overall seepage activity in May 2016 compared to a survey in the same area in August 2012 (Table 1), consistent with cold-seep hibernation during the cold season. While we do not have direct evidence for the expected shoaling of gas flare positions during summertime, we observed highest increase of flare abundance in the shallower parts of the depth interval in which the GHSZ fluctuates as a function of seasonal temperature variations (360-410 m) (Figs. 2 and 3). This agrees with a shift of the limit of the GHSZ towards deeper water depth and a depletion of the benthic gas hydrate capacitor during the warm season. However, seasonal temperature fluctuations penetrate generally less than 5-10 m into the sediments[31,42]. While the gas hydrate capacitor in shallow sediments is influenced by seasonal temperature variations, gas hydrate dynamics within deeper sediments are likely not affected by seasonal temperature variations. However, in a warming Arctic, it is most likely that the GHSZ will shift to deeper areas, potentially exposing areas where hydrates are permanently stable at present-day temperature conditions.

We also demonstrate that the seep-associated MOx in the water column slows down by 2-3 orders of magnitude (i.e. < 0.001 nmol l^{-1} d^{-1} on average in May 2016 compared to 0.34 nmol l^{-1} d^{-1} on average in August 2012 (ref. 19), Table 1, Extended Data Fig. 4) during cold-seep hibernation when water column CH_4 concentrations are about tenfold lower compared to summertime conditions (Fig. 3). Previous studies have shown a similar non-linear relationship between MOx and CH_4 concentrations with a drop of MOx by 3 orders magnitude related to a decrease of CH_4 concentrations by only one order of magnitude[19,21]. Temperature alone was

found to lead to changes in MOx by a factor of 1.5-5 per 10 °C (ref. 46) and thus seems to only play a minor role in modifying microbial methanotrophy in the water column of the study area. Similar to MOx, seasonal temperature variation will also only have a relatively small effect on the anaerobic oxidation of methane (AOM – not measured during our expeditions) in sediments (factor of ~2 per 10 °C, ref. 47, 48), so that variations in AOM will, likely, not substantially influence methane release rates from the sediments in the study area.

Seasonal bottom-water temperature fluctuations of 2-3 °C (ref. 49) at the depth of the gas hydrate stability limit are common at latitudes above 65°N (Fig. 4 and Extended Data Fig. 5). We argue that solely relying on data obtained during summer when calculating annual rates of CH_4 release from sediments in high-latitude environments will unequivocally lead to overestimates by at least 30 %. Assuming a steady methane release coupled to the steady temperature increase detected in the area at the MASOX site (MASOX = Monitoring Arctic Seafloor-Ocean Exchange observatory[26]), and considering the cold-season fluxes determined here translates to a total CH_4 release along our 11 km area along the continental margin of 2,120 mol CH_4 $^{-1}$ yr^{-1} m^{-1} (cf. Extended Data Fig. 6 for comparison with fluxes estimated from summer surveys). Spatial extrapolation along the 360 m isobaths at the Norwegian-western Svalbard margin (the hotspot for future CH_4 release in the Arctic[50], total length ~6,360 km, Fig. 4) yields a minimum of 1.4 giga mol CH_4 per year liberated to the water column. The future evolution of the size of the gas hydrate reservoir offshore Svalbard is still uncertain[31], making predictions on the development of cold seep hibernation in a warming ocean extremely challenging. Our findings highlight the necessity to account for seasonal cyclicity in future assessments of regional and global CH_4 budget from marine methane seeps.

References

1. Edenhofer, O. *Climate Change 2014: Mitigation of Climate Change : Summary for Policymakers* (Intergovernmental Panel on Climate Change, 2014).

2. Etminan, M., Myhre, G., Highwood, E. J. & Shine, K. P. Radiative forcing of carbon dioxide, methane, and nitrous oxide: A significant revision of the methane radiative forcing. *Geophys. Res. Lett.* **43,** 12,614-612,623 (2016).

3. Myhre, C. L. et al. Monitoring of greenhouse gases and aerosols at Svalbard and Birkenes in 2015 - Annual report. (Miljødirektoratet rapport, M-454/2015, NILU, 2016).

4. Kirschke, S. et al. Three decades of global methane sources and sinks. *Nat. Geosci.* **6,** 813 (2013).

5. Kvenvolden, K. A. Methane hydrate — A major reservoir of carbon in the shallow geosphere? *Chem. Geol.* **71,** 41-51 (1988).

6. Hunter, S. J., Goldobin, D. S., Haywood, A. M., Ridgwell, A. & Rees, J. G. Sensitivity of the global submarine hydrate inventory to scenarios of future climate change. *Earth Planet. Sci. Lett.* **367,** 105-115 (2013).

7. Kretschmer, K., Biastoch, A., Rüpke, L. & Burwicz, E. Modeling the fate of methane hydrates under global warming. *Global Biogeochem. Cycles* **29,** 610-625 (2015).

8. Shakhova, N. et al. Extensive Methane Venting to the Atmosphere from Sediments of the East Siberian Arctic Shelf. *Science* **327,** 1246-1250 (2010).

9. Ruppel, C. Permafrost-Associated Gas Hydrate: Is It Really Approximately 1 % of the Global System? *J. Chem. Eng. Data* **60,** 429-436 (2015).

208 10. Kvenvolden, K. A. A review of the geochemistry of methane in natural gas hydrate. *Org.*
209 *Geochem.* **23,** 997-1008 (1995).

210 11. Vadakkepuliyambatta, S., Chand, S. & Bünz, S. The history and future trends of ocean
211 warming-induced gas hydrate dissociation in the SW Barents Sea. *Geophys. Res. Lett.* **44,**
212 835-844 (2017).

213 12. Andreassen, K. et al. Massive blow-out craters formed by hydrate-controlled methane
214 expulsion from the Arctic seafloor. *Science* **356,** 948-953 (2017).

215 13. Serov, P. et al. Postglacial response of Arctic Ocean gas hydrates to climatic
216 amelioration. *Proc. Nat. Acad. Sci.* **114,** 6215-6220 (2017).

217 14. Overland, J. E., Wang, M., Walsh, J. E. & Stroeve, J. C. Future Arctic climate changes:
218 Adaptation and mitigation time scales. *Earth's Future* **2,** 68-74 (2014).

219 15. Rosenthal, Y., Linsley, B. K. & Oppo, D. W. Pacific Ocean Heat Content During the Past
220 10,000 Years. *Science* **342,** 617-621 (2013).

221 16. Ferré, B., Mienert, J. & Feseker, T. Ocean temperature variability for the past 60 years on
222 the Norwegian-Svalbard margin influences gas hydrate stability on human time scales. *J.*
223 *Geophys. Res-Oceans* **117,** C10017 (2012).

224 17. Treude, T., Krüger, M., Boetius, A. & Jørgensen, B. B. Environmental control on
225 anaerobic oxidation of methane in the gassy sediments of Eckernförde Bay (German
226 Baltic). *Limnol. Oceanogr.* **50,** 1771-1786 (2005).

227 18. Reeburgh, W.S. Oceanic Methane Biogeochemistry. *Chem. Rev.* **107,** 486-513 (2007).

19. Steinle, L. et al. Water column methanotrophy controlled by a rapid oceanographic switch. *Nature Geosci.* **8,** 378-382 (2015).

20. Crespo-Medina, M. et al. The rise and fall of methanotrophy following a deepwater oil-well blowout. *Nat. Geosci.* **7,** 423 (2014).

21. James, R. H. et al. Effects of climate change on methane emissions from seafloor sediments in the Arctic Ocean: A review. *Limnol. Oceanogr.* **61,** S283-S299 (2016).

22. Appen, W.-J. v., Schauer, U., Hattermann, T. & Beszczynska-Möller, A. Seasonal Cycle of Mesoscale Instability of the West Spitsbergen Current. *J. Phys. Oceanogr.* **46,** 1231-1254 (2016).

23. Beszczynska-Möller, A., Fahrbach, E., Schauer, U. & Hansen, E. Variability in Atlantic water temperature and transport at the entrance to the Arctic Ocean, 1997–2010. *ICES J. Mar. Sci.* **69,** 852-863 (2012).

24. Phrampus, B. J. & Hornbach, M. J. Recent changes to the Gulf Stream causing widespread gas hydrate destabilization. *Nature* **490,** 527 (2012).

25. Marín-Moreno, H., Minshull, T. A., Westbrook, G. K., Sinha, B. & Sarkar, S. The response of methane hydrate beneath the seabed offshore Svalbard to ocean warming during the next three centuries. *Geophys. Res. Lett.* **40,** 5159-5163 (2013).

26. Berndt, C. et al. Temporal constraints on hydrate-controlled methane seepage off Svalbard. *Science* **343**, 284-287 (2014).

247 27. Knies, J., Damm, E., Gutt, J., Mann, U. & Pinturier, L. Near-surface hydrocarbon
248 anomalies in shelf sediments off Spitsbergen: Evidences for past seepages. *Geochem.*
249 *Geophys. Geosyst.* **5** (2004).

250 28. Damm, E., Mackensen, A., Budéus, G., Faber, E. & Hanfland, C. Pathways of methane in
251 seawater: Plume spreading in an Arctic shelf environment (SW-Spitsbergen). *Cont. Shelf*
252 *Res.* **25,** 1453-1472 (2005).

253 29. Westbrook, G. K. et al. Escape of methane gas from the seabed along the West
254 Spitsbergen continental margin. *Geophys. Res. Lett.* **36** (2009).

255 30. Sahling, H. et al. Gas emissions at the continental margin west of Svalbard: mapping,
256 sampling, and quantification. *Biogeosciences* **11,** 6029-6046 (2014).

257 31. Wallmann, K. et al. Gas hydrate dissociation off Svalbard induced by isostatic rebound
258 rather than global warming. *Nat. Commun.* **9,** 83 (2018).

259 32. Mau, S. et al. Widespread methane seepage along the continental margin off Svalbard -
260 from Bjornoya to Kongsfjorden. *Sci. Rep.* **7,** 42997 (2017).

261 33. Panieri, G., Graves, C. A. & James, R. H. Paleo-methane emissions recorded in
262 foraminifera near the landward limit of the gas hydrate stability zone offshore western
263 Svalbard. *Geochem. Geophys. Geosyst.* **17,** 521-537 (2016).

264 34. Veloso, M., Greinert, J., Mienert, J. & De Batist, M. A new methodology for quantifying
265 bubble flow rates in deep water using splitbeam echosounders: Examples from the Arctic
266 offshore NW-Svalbard. *Limnol. Oceanog.-Meth.* **13,** 267-287 (2015).

35. Graves, C. A. et al. Methane in shallow subsurface sediments at the landward limit of the gas hydrate stability zone offshore western Svalbard. *Geochim. Cosmochim. Ac.* **198,** 419-438 (2017).

36. Myhre, C. L. et al. Extensive release of methane from Arctic seabed west of Svalbard during summer 2014 does not influence the atmosphere. *Geophys. Res. Lett.* **43,** 4624-4631 (2016).

37. Feseker, T. et al. Eruption of a deep-sea mud volcano triggers rapid sediment movement. *Nat. Commun.* **5,** 5385 (2014).

38. Boles, J. R., Clark, J. F., Leifer, I. & Washburn, L. Temporal variation in natural methane seep rate due to tides, Coal Oil Point area, California. *J. Geophys. Res.-Oceans* **106,** 27077-27086 (2001).

39. Römer, M., Riedel, M., Scherwath, M., Heesemann, M. & Spence, G. D. Tidally controlled gas bubble emissions: A comprehensive study using long-term monitoring data from the NEPTUNE cabled observatory offshore Vancouver Island. *Geochem. Geophys. Geosyst.* **17,** 3797-3814 (2016).

40. Franek, P. et al. Microseismicity Linked to Gas Migration and Leakage on the Western Svalbard Shelf. *Geochem. Geophys. Geosyst.* **18,** 4623-4645 (2017).

41. Sarkar, S. et al. Seismic evidence for shallow gas-escape features associated with a retreating gas hydrate zone offshore west Svalbard. *J. Geophys. Res.* **117,** 9102 (2012).

42. Riedel, M. et al. Distributed natural gas venting offshore along the Cascadia margin. *Nat. Commun.* **9** (2018).

43. Thatcher, K. E., Westbrook, G. K., Sarkar, S. & Minshull, T. A. Methane release from warming-induced hydrate dissociation in the West Svalbard continental margin: Timing, rates, and geological controls. *J. Geophys. Res.-Solid Earth* **118,** 22-38 (2013).

44. Anderson, B. et al. in *Proceedings of the 8th international conference on gas hydrates (ICGH8-2014).*

45. Dickens, G. On the fate of past gas: What happens to methane released from a bacterially mediated gas hydrate capacitor? *Geochem. Geophy. Geosy.* **2** (2001).

46. Segers, R. Methane Production and Methane Consumption: A Review of Processes Underlying Wetland Methane Fluxes. *Biogeochemistry* **41,** 23-51 (1998).

47. Nauhaus, K., Treude, T., Boetius, A. and Kruger, M.: Environmental regulation of the anaerobic oxidation of methane: a comparison of ANME-I and ANME-II communities, *Environ. Microbiol.*, **7,** 98–106 (2005)

48. Holler, T., et al. Thermophilic anaerobic oxidation of methane by marine microbial consortia, *ISME J.*, **5,** 1946–1956 (2011)

49. Boyer, T. P. et al. World Ocean Database 2009. 216 (NOAA Atlas NESDIS 66, U.S. Gov., Wash., D.C., 2009).

50. Vadakkepuliyambatta, S. et al. Climatic impact of Arctic Ocean methane hydrate dissociation in the 21st-century. *Earth Syst. Dynam. Discuss.* 2017, 1-27, doi:10.5194/esd-2017-110 (2017).

Acknowledgments: We would like to thank the crew of R/V Helmer Hanssen during the survey CAGE 16-4. The authors thank the late Heiko Sahling for invaluable input. This study is a part of CAGE (Centre for Arctic Gas Hydrate, Environment and Climate), Norwegian Research Council grant no. 223259).

Author contributions: B.F. and H.N. designed the study. B.F wrote the manuscript in close collaboration with H.N, and with input from P.J., M.M., P.S., C.G., A.P., C.B., G.P. and M.F.L. P.J. and M.M. provided the details and calculations of methane flow rates. P.S and C.G provided the methane measurements. F.G and H.N. provided the MOx measurements.

Competing interests: The authors declare no competing interests.

Data and materials availability: Bottom-water temperatures are accessible from the NOAA-NODC website (https://www.nodc.noaa.gov/OC5/WOD13/). All data needed to evaluate the conclusions in the paper are present in the paper and/or the Supplementary Materials. Additional data are available on the platform Open research Data at the University of Tromsø – The Arctic University of Norway (https://doi.org/10.18710/EIFZ2J).

Figures and Tables Captions:

Fig. 1. Bathymetric map of the study area. a) Flare locations are indicated as yellow (cold season, May, 2016) and red dots (warm season, August 2012, ref. 30). The modelled limits of the Gas hydrate stability zone (GHSZ) at 1.5 and 3 °C bottom-water temperature are also indicated (blue and white lines), as well as the MASOX (Monitoring Arctic Seafloor – Ocean Exchange) water sampling transects (dashed white line). b) Ship track during CAGE 16-4 (May 2016 on-board R/V *Helmer Hanssen*) (black line), with flares detected during the cruise (yellow dots). c) General map of the study area.

Fig. 2. Flare density during warm and cold bottom-water conditions. a) Number of flares in 2 m-depth intervals during the He-387 survey during the warm season (August 2012, red[30]) and during the CAGE 16-4 survey during the cold season (May 2016, yellow) in the study area b) Percent difference in flare density from warm to cold season. The figure highlights the overall decrease of flare density, in particular in shallow waters during the cold season. Note that darker yellow results from superimposing warm (red) and cold (yellow) seasons.

Fig. 3. Cross-section schematic of the temporal variation of the GHSZ. The seasonal shift of the GHSZ is illustrated by a) strong reduction in CH_4 seepage and MOx activity during cold seasons compared to b) usually activity of CH_4 seepage and MOx during warm seasons. Indicated depths of GHSZ were estimated by Berndt et al.[26].

Fig. 4. Interpolated bottom-water temperature distribution in the Arctic a) January to April (cold season), b) July to October (warm season). The figure highlights seasonal temperature variation between both seasons. Hotspots for future methane release in the Arctic are anticipated along the 360 m isobaths (thick black dotted line)[50]. The black rectangle shows the area used in our calculation for potential methane release in the Norwegian/Svalbard margin along the 360 m isobaths (see Extended Data Fig. 5). The known methane seepages sites (ref. 50 and references therein) are shown as black triangles. Data source: NODC, maximum 25 meters above the seafloor.

Table 1. Comparison of water column analysis between warm and cold conditions. Warm conditions are based on *Sahling et al.[30] observed 30 August 2012, and **Steinle et al.[19] observed 18-19 and 30-31 August 2012. Summertime FlareHunter estimate (✢) is calculated from the Sahling et al.[30] results by applying a correction factor corresponding to the ratio between the FlareHunter and Sahling et al.[30] results for the data from cold condition.

354 **Methods**

355 **Study design**

356 We analysed the seasonal variability of CH_4 seepage between warm and cold bottom-water
357 conditions, and conducted a 1,032 m-long hydro-acoustic survey (CAGE 16-4 survey, R/V
358 *Helmer Hanssen*, May 1st to 9th, 2016) at the upper limit of the GHSZ (~390 m water depth;
359 Fig. 1) during cold bottom-water conditions. Our survey fully overlapped with a ~30 km^2 area
360 previously investigated for CH_4 emissions by Sahling et al.[30] in late summer 2012, when
361 bottom water was comparably warm. We compared the position and density of flares detected
362 between these two surveys. Accounting for differences in ship track and overlapping flare
363 observations, we calculated the number of hydro-acoustically detected flares. In addition, we
364 performed two transects (five sampling stations each) with CTD (conductivity, temperature,
365 depth) casts and water column sampling for CH_4 concentration and measurements of aerobic
366 oxidation rates of CH_4 (MOx - see method section) at positions crossing the MASOX site
367 (MASOX = Monitoring Arctic Seafloor-Ocean Exchange observatory[26]) (Fig. 1). The distance
368 between stations was ~500 m on May 6th and ~250 m on May 8th. The locations of transect
369 lines and hydrocasts performed in this study match the sampling scheme of Steinle et al.[19] in
370 August 2012, allowing comparison of water column CH_4 concentrations and MOx rates
371 between the cold and warm seasons.

372 **Enumeration of flares**

373 CH_4 ebullition from the seafloor was detected as acoustic flares with a single beam echo
374 sounder system (Simrad EK60) at 38 KHz (e.g. 30,32) during the CAGE 16-4 cruise
375 conducted in May 2016. The flare distribution from this survey was compared with data from
376 late summer 2012 (R/V *Heincke* cruise He-387), which carried a similar echosounder
377 system[30].

For comparison between the two surveys, we considered flares detected in May (2016) and those previously mapped in August (2012) in the commonly surveyed area of ~30 km^2 (termed Area 3 in Sahling et al.[30]) at the upper continental slope near ~400 m water depth. Our echosounder has a swath angle of 6.81° (at 38 kHz), and a footprint which accordingly covers ~47 m of seabed at ~400 m water depth. We only compared those flares from Sahling et al.[30] that were within +/- 23.5 m from our ship track. In order to avoid counting the same flare more than once (e.g. some flares were detected multiple times as they rose at an angle through the water column), we counted only a maximum of one flare within each 50 m radius (Extended Data Fig. 1).

Flow-rate estimates

The FlareHunter software was used to convert raw echosounder data from the EK60 to beam-compensated target strength, which is proportional to the amount of gas bubbles in the water column[34]. We manually distinguished flares from noise (i.e. fish, seafloor, and interferences) and isolated a 5 m thick layer from 5 to 10 meters above the seafloor. This depth interval was selected because it is close to the bubble source, but excludes reverberation effects from the seafloor. Overlapping flares within the echosounder coverage at the seafloor were clustered using the FlareHunter clustering algorithm and we subsequently used the FlareFlowModule embedded in the FlareHunter software to calculate flow rates[34]. As boundary conditions, we used in situ temperatures and hydrostatic pressure from CTD casts. We assumed a Gaussian-type bubble size distribution, and used an average flow rate from seven different bubble rising speed models[34].

Biogeochemistry of the water column

Water column sampling – We used a 12 × 5-liter CTD (SBE 911plus)/Rosette sampler to recover samples form discrete water depth. Seawater subsamples for CH_4 concentration and MOx rate measurements were taken immediately upon recovery of the rosette.

Methane concentrations – CH_4 was measured using a conventional headspace method[Error! Reference source not found.]. Water samples were collected bubble free into 120 mL crimp seal bottles and fixed with 1 mL of 1 M NaOH solution. In exchange with sampled water 5 ml of nitrogen gas was added and the bottles were vigorously shaken for 2 minutes to facilitate equilibration of dissolved and headspace gas. Bottles were kept in the refrigerator (5 °C) until analysis within a few hours after sampling. Equilibrated headspace gas (100 µl) was analysed by gas chromatography with flame ionisation detection (ThermoScientific Trace 1310 equipped with a TG-BOND Msieve 5A column, operated isothermally at 150°C with 20 ml min^{-1} H_2 carrier gas).

MOx rates – MOx rates were measured directly from ex-situ incubations with trace amounts of tritium- labelled CH_4 ($C\ ^3H_4$), allowing tracing of ^3H-labelled transfer from the substrate to the MOx product pool by measurement of the activities of the produced ^3H_2O as well as total activity (residual C^3H_4 and produced ^3H_2O) after incubation. MOx rates were measured according to a previously published method[19,Error! Reference source not found.] with modifications. Briefly, hexaplicates of seawater was subsampled to fill 20 ml crimp seal serum vials, capped with bromobutyl rubber stoppers that do not impede MOx activity[Error! Reference source not found.], amended with trace amounts of C^3H_4 (10 µl gaseous C^3H_4/N_2, ~25 kBq, <50 pmol CH_4, American Radiolabeled Chemicals, USA) and incubated for 72h at in-situ temperature in the dark. The incubations were terminated in two ways for measuring ^3H_2O and total activity, respectively. For measurements of ^3H_2O activity, we terminated one incubation triplicate by unsealing it and stripping out residual C^3H_4 by purging the samples with air. An aliquot of 10

ml of stripped sample was then kept cool in a closed 20 ml polyethylene scintillation vial until measurement of ^3H_2O in our laboratory at the Department of Geoscience, The Arctic University of Norway. For total activity, incubations of the remaining triplicate were terminated/fixed by injecting 0.5 ml saturated $HgCl_2$ solution into the samples on board until further processing on land. Directly after the cruise, (i) total and (ii) ^3H_2O activity were measured by wet scintillation counting. For this, 10 ml of scintillation cocktail (Ultima Gold, Perkin Elmer) were mixed with (i) the 10 ml of the purged sample, and ^3H_2O activity was measured with a Packard Packard Tricarb 2300 TR scintillation counter (Perkin Elmer, USA). Similarly, the (ii) triplicate of $HgCl_2$-fixed sample was uncapped and 10 ml were immediately mixed with 10 ml scintillation cocktail for measuring total activity. MOx rates were then calculated from the fractional turnover of labelled CH_4 assuming first order kinetics[18]:

$$rMOx = {}^3H_2O \times ({}^3H_2O + C^3H_4)^{-1} \times [CH_4] \times t^{-1} \quad (1)$$

where ^3H_2O and C^3H_4 are the activities of the produced ^3H_2O and residual C^3H_4, respectively, $[CH_4]$ is the CH_4 concentration and t is the incubation time. All incubations were corrected for (insubstantial) tracer turnover in killed controls[19,**Error! Reference source not found.**].

Estimate of total annual methane release

To estimate the total annual CH_4 release, we considered the study area, 11 km stretch along the continental margin[30], from where 58 mol CH_4 min^{-1} are released from the sediment during the six warmer months, contrasting 33 mol CH_4 min^{-1} (i.e. 43% less) during the six colder months. Assuming that the situation along the 11 km offshore Svalbard is representative of the Arctic Margin, we extrapolated our estimates to the Norwegian-Western Svalbard margin along the 360 m isobath (total length = ~6,360 km), which is considered as a hotspot for future CH_4 release[50] (c.f. black rectangle in Fig. 4 and Extended Data Fig. 5).

447 Our estimate of how much methane budgets which neglect the seasonal variation in CH_4
448 fluxes overestimate actual methane release was calculated as follows. If all months of the year
449 are assumed to have the same methane flux, which is based on summertime observations:
450 $FA_{(previous\ estimates)} = 12 \cdot FMw$, where FA is the annual flux and FMw is the monthly flux for a
451 warm month. Wintertime flux observations allow a more realistic annual flux estimate: $FA_{(new}$
452 $_{estimate)} = 6 \cdot FMw + 6 \cdot FMc$, where FMc is the monthly flux for a cold month. Our results show
453 that the wintertime flux is a 43 % reduction of the summertime flux, such that: $FMc = FMw -$
454 $0.43 \cdot FMw$. The overestimation of previous estimates compares to our new estimate is
455 therefore given by:

456 $$\left|\frac{FA_{(previous\ estimates)} - FA_{(new\ estimate)}}{FA_{(new\ estimate)}}\right| = \left|\frac{12 \cdot FMw - (6 \cdot FMw + 6 \cdot FMc)}{(6 \cdot FMw + 6 \cdot FMc)}\right| \approx 30\ \%$$

457 Although the real seasonal temperature variation is sinusoidal-like, and therefore only
458 extremely roughly represented by 6 warm months and 6 cold months, the model presented
459 above represents the limitations of available observations. Previous estimates based on a
460 single observations were forced to assume that all months were the same. By adding
461 wintertime observations, our study allows this model to be improved to incorporate the two
462 observed states of the system.

463 Reference methods

464 51. Kolb, B. & Ettre, L. S. Static Headspace-Gas Chromatography: Theory and Practice.
465 (John Wiley & Sons, Inc, Hoboken, NJ, USA, 2006).

466 52. Niemann, H. et al. Toxic effects of lab-grade butyl rubber stoppers on aerobic methane
467 oxidation. *Limnol. Oceanog.-Meth* **13**, 40-52 (2015).

468

Fig. 1

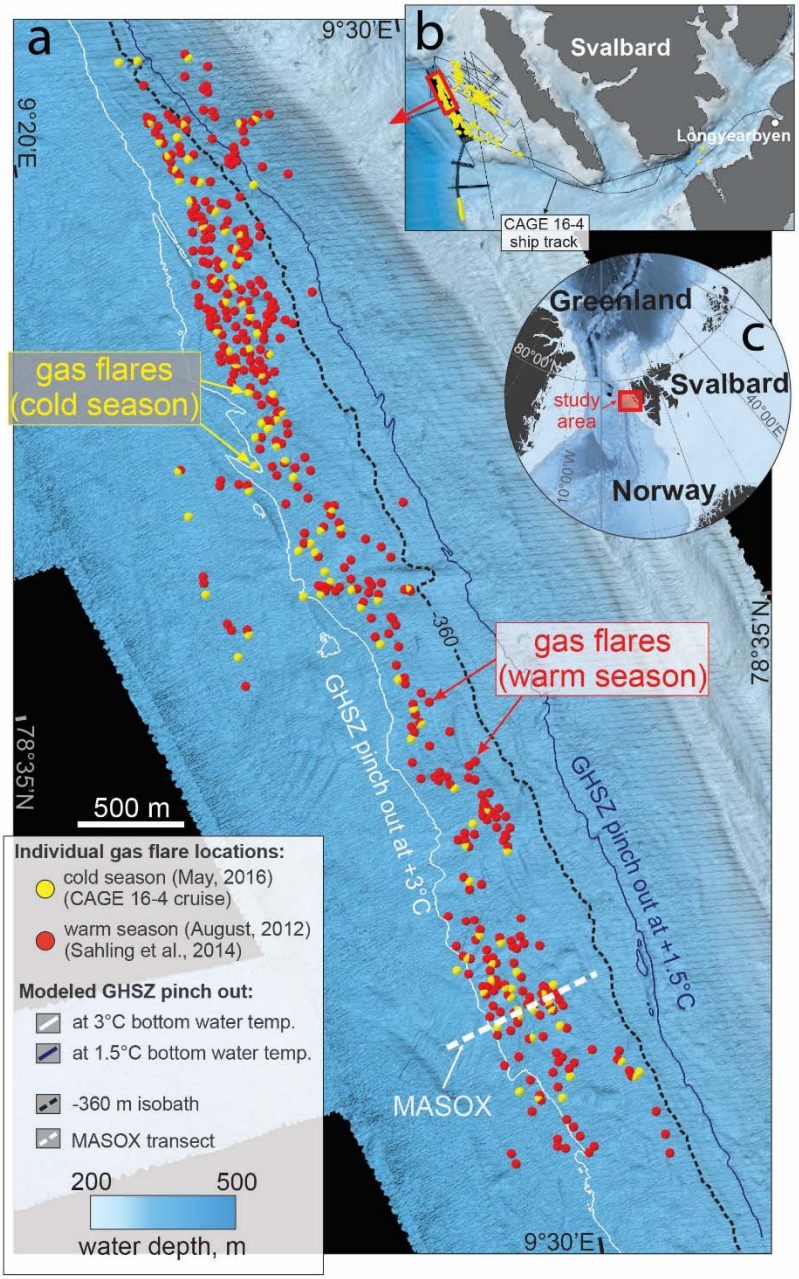
a
9°30'E
9°20'E
78°35'N
b
Svalbard
Longyearbyen
CAGE 16-4
ship track
Greenland
c
80°00'N
Svalbard
study
area
40°00'E
10°00'W
Norway
gas flares
(cold season)
gas flares
(warm season)
360
GHSZ pinch out at +3°C
GHSZ pinch out at +1.5°C
MASOX
500 m
Individual gas flare locations:
cold season (May, 2016)
(CAGE 16-4 cruise)
warm season (August, 2012)
(Sahling et al., 2014)
Modeled GHSZ pinch out:
at 3°C bottom water temp.
at 1.5°C bottom water temp.
-360 m isobath
MASOX transect
200
500
water depth, m

469

470

Fig. 2

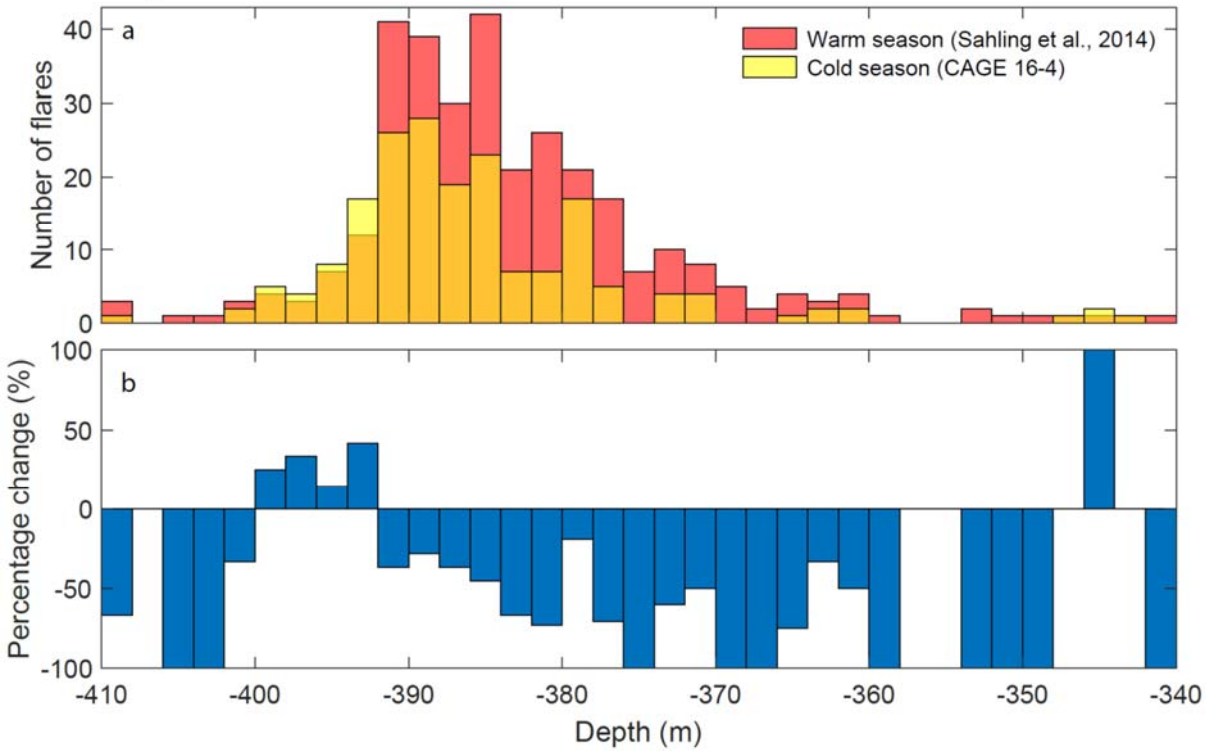

471

472 Fig. 3

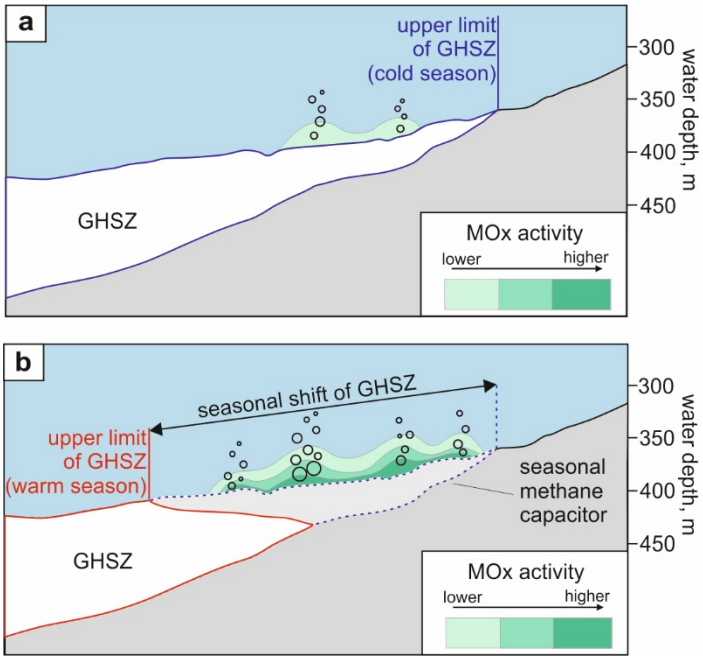

473

Fig. 4

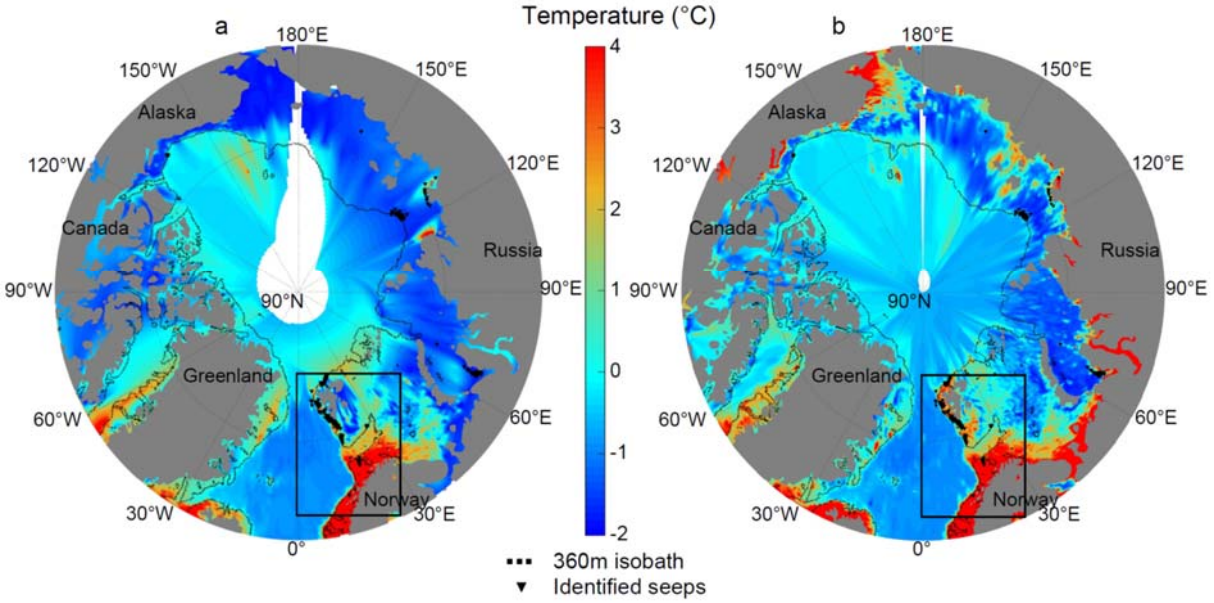

474

Table 1

Description	Warm condition	Cold condition (this study)
Number of flares	344 (*)	196
Flow rate based on Sahling et al. method[30] (mol CH_4 min^{-1})	77 (*)	44
Flow rate estimated with FlareHunter (mol CH_4 min^{-1})	58 (+)	33
Average temperature at the seafloor (°C)	3.5 (**)	1.7 ± 0.1
Salinity range in the water column (PSU)	~34.5 (**)	34.9 ± 0.01
Average CH_4 in the water column (nmol l^{-1})	~25 (**)	4.8 ± 11.07
Maximum CH_4 near the seafloor (nmol l^{-1})	> 400 (**)	111
Maximum MOx in MASOX transect (nmol l^{-1} d^{-1})	~3 (**)	0.001
Average MOx in MASOX transect (nmol l^{-1} d^{-1})	0.34 (**) ± 0.06	0.001 ± 0.002
Total MOx in the study area of 30 km^2 (mol min^{-1})	2.8 (**) ± 0.48	0.01 ± 0.02

475

476 **Supplementary Information for:**

477 **Reduced methane seepage from Arctic sediments during cold bottom water conditions**

478 Bénédicte Ferré[1*], Pär G. Jansson[1], Manuel Moser[1], Pavel Serov[1], Alexey Portnov[1,2], Carolyn
479 Graves[3,4], Giuliana Panieri[1], Friederike Gründger[1], Christian Berndt[5], Moritz F. Lehmann[6,],
480 Helge Niemann[1,6,7,8]

481 * Correspondence to: benedicte.ferre@uit.no

482 [1]CAGE-Centre for Arctic Gas Hydrate, Environment and Climate, Department of
483 Geosciences, The Arctic University of Norway, 9037 Tromsø, Norway.

484 [2]School of Earth Sciences, The Ohio State University, Columbus, Ohio 43210, USA.

485 [3]Baltic Sea Research Institute, IOW, 18119 Rostock-Warnemuende, Germany.

486 [4]Currently at Centre for Environment, Fisheries and Aquaculture Science (Cefas), Lowestoft,
487 Suffolk, NR33 0HT, UK.

488 [5]GEOMAR Helmholtz Centre for Ocean Research Kiel, 24148 Kiel, Germany.

489 [6]Department of Environmental Science, University of Basel, 4056 Basel, Switzerland.

490 [7]NIOZ Royal Netherlands Institute for Sea Research, Department of Marine Microbiology &
491 Biogeochemistry, and Utrecht University, Landsdiep 4, 1797 SZ 't Horntje, the Netherlands

492 [8]Department of Earth Sciences, Faculty of Geosciences, Utrecht University, 3508 TC Utrecht,
493 the Netherlands

S.I.1. Enumeration of flares and flow-rates estimates

The filtering method as illustrated in supplementary Fig. 1 revealed highly variable flow rates between flare clusters, ranging from 2 to 1,900 ml min^{-1} (Supplementary Fig. 2), and results in flow rates of ~2,140 mol CH_4 $^{-1}$ yr^{-1} m^{-1}. The averaged quantified volume flux of 20.9 mL min^{-1} estimated by Sahling et al. (ref. 30) translate to an averaged mass flux of 37.1 mmol min^{-1} assuming pure CH_4. Using only the 344 flares observed by Sahling et al. (ref. 30) which overlapped with our surveyed area, we calculated a total CH_4 release per year of 3,700 mol CH_4 $^{-1}$ yr^{-1} m^{-1} in the section.

S.I.2. Water column biogeochemistry

The water column biogeochemistry is shown in Supplementary Fig. 3, along with temperature and salinity.

In addition to a springtime reduction in flare numbers, lower CH_4 release to the water column, and lower water column CH_4 contents, we also observed a strong reduction in MOx activity. Oceanographic conditions during our 2016 survey (low bottom water temperature of < 2 °C; high salinity of ~ 35.1 PSU) suggest a weak mode of the West Spitzbergen Current (WSC), which has been previously linked to enhanced water column methanotrophic activity in this area[19]. Yet, the MOx rates (on average < 0.001 nmol l^{-1} d^{-1} across the MASOX site) were three orders of magnitude lower than those observed during a similar current regime in summer of 2012. Across the MASOX site, this was 0.54 nmol l^{-1} d^{-1} on average on August 18/19 2012, and 0.34 nmol l^{-1} d^{-1} on average during the entire observation period in August 2012 (including offshore and onshore modes of the WSC)[19] (Table 1, Supplementary Fig. 4). The overall low MOx rate, despite favourable oceanographic conditions, suggest that MOx was modulated by other environmental conditions, probably low CH_4 availability[21].

S.I.3. Discussion on potential impact on methane fluxes to the atmosphere

As of today, several studies conducted close to our study area (in summertime) showed that rather minor amounts of methane are released to the atmosphere[4,5]. Under less stratified conditions in wintertime, at least in shallow water, one can expect that methane that has not been consumed by bacteria will more likely reach the atmosphere (e.g. 8). We did not conduct sea-atmosphere flux measurements during our campaigns. Nevertheless, our results demonstrate that the water column was depleted in methane during cold bottom-water temperature conditions (<1 nM at the surface, atmospheric equilibrium concentration ~4 nM). Hence, it appears that, if at all, only small amounts of methane in our study area reach the atmosphere during wintertime. It is also important to add that our study area is > 350 m depth, providing more time for methane utilisation by microbes before reaching the sea-surface than at shallow water sites such as in Shakhova et al. (ref. 8) or Steinle et al. (ref. 7).

S.I.4. Interpolated bottom water temperature along the Norwegian-Svalbard margin

Supplementary Fig. 6 shows the bottom water temperature represented in the white rectangle in Fig. 3.

S.I.5. Comparison of annual fluxes with literature

We compare our estimated annual flux with previous studies in the same area, all occurring during warm bottom water temperature conditions (supplementary Table 1). We translate our unit to mol CH_4 yr^{-1} to cover the entire areas corresponding to each study. We used here a total of 344 flares for comparison with Sahling et al. (ref. 30). Flow rate by Veloso et al. (ref. 8) was taken from an area between 78°38'30''-78°40'N and 9°23'- 9°28' E, at ~ 240m depth. Jansson et al. (ref. 9) estimated the flow rate above a reduced area of 4.5 km along the MASOX site where they found 68 flares, explaining their low number. Veloso-Alarcón et al. (ref. 10) compiled 9 echosounder surveys in and around our area, covering water depths of

194 – 410 m. Based on this table, the methane flux estimated in this study is lower than previously estimated from summer surveys.

S.I.6. CTD data

Supplementary Table 2 shows the CTD data along the MASOX site. Parameters are indicated on the first line.

References

1. Sahling, H. et al. Gas emissions at the continental margin west of Svalbard: mapping, sampling, and quantification. *Biogeosciences* **11,** 6029-6046 (2014).
2. Steinle, L. et al. Water column methanotrophy controlled by a rapid oceanographic switch. *Nature Geosci.* **8,** 378-382 (2015).
3. James, R. H. et al. Effects of climate change on methane emissions from seafloor sediments in the Arctic Ocean: A review. *Limnol. Oceanogr.* **61,** S283-S299 (2016).
4. Gentz, T., et al. A water column study of methane around gas flares located at the West Spitsbergen continental margin. *Cont. Shelf Res.* **72**(Supplement C):107-18 (2014)
5. Myhre, C.L. et al. Extensive release of methane from Arctic seabed west of Svalbard during summer 2014 does not influence the atmosphere. *Geophys. Res. Lett.* **43,** 4624-31 (2016)
6. Shakhova, N. et al. Extensive Methane Venting to the Atmosphere from Sediments of the East Siberian Arctic Shelf. *Science* **327,** 1246-1250 (2010).
7. Steinle, L. et al. Effects of low oxygen concentrations on aerobic methane oxidation in seasonally hypoxic coastal waters. *Biogeosciences* **14,** 2017;

8. Veloso, M., Greinert, J., Mienert, J. and De Batist, M. A new methodology for quantifying bubble flow rates in deep water using splitbeam echosounders: Examples from the Arctic offshore NW-Svalbard. *Limnol. Oceanogr. Methods* **13**: 267-287 (2015)

9. Jansson, P. et al. High-resolution underwater laser spectrometer sensing provides new insights into methane distribution at an Arctic seepage site. *Ocean Sci.* **15**, 1055-1069 (2019).

10. Veloso-Alarcón, M. E. et al. Variability of Acoustically Evidenced Methane Bubble Emissions Offshore Western Svalbard. *Geophys. Res. Lett.* **46**, 9072-9081 (2019)

11. Berndt, C. et al. Temporal constraints on hydrate-controlled methane seepage off Svalbard. *Science* **343**, 284-287 (2014)

Supplementary Figure Captions:

Supplementary Fig. 1: **Ship track (purple line) and flare locations during CAGE 16-4 (yellow dots) and from He-387 survey[30] (red dots)** a) before and b) after application of filtering procedure. The insets are zoomed area from the white rectangle (c) before filter, d) after filter). The size of the circles in the insets represents the 50 m diameter overlap limit imposed for individual flares. The green area around the ship track the echosounder footprint accounting for the swath angle and the pitch and roll of the ship. He-387 survey lines achieve ~100 % of the area and are therefore not shown.

Supplementary Fig. 2. **CAGE 16-4 methane flow rates calculated with the FlareHunter software.** Both ship tracks (He-387[30], red line and CAGE 16-4, grey line) are represented.

Supplementary Fig. 3. **Water column biogeochemistry across the MASOX site.** Distribution of methane (upper panels), potential temperature (middle panels) and salinity

(lower panels) on May 6th (a-c) and May 8th 2016 (d-f) (see Fig. 1 for transect location). Position of discrete samples are indicated by circles.

Supplementary Fig. 4. **Comparison of MOx rates measured at the MASOX station between warm and cold seasons**. Warm seasons (red) are based on the average observations by Steinle et al.[19] in August 2012 – which we binned in 50 m intervals. Rates from May 2016 are indicated in yellow. Error bars are based on the standard deviation from the replicates analysis at each given depth/bin (n>6). Note the broken x-axis, highlighting the dramatic reduction of MOx rate during cold season.

Supplementary Fig. 5: **Interpolated bottom water temperature along the Norwegian-Svalbard margin** (zoom-in of rectangle in Fig. 3). Colour code and legend are the same as in Fig. 3. The 2 °C isotherm (temperature corresponding to the 3-phase equilibrium at 360 m depth) is represented by the white line. a) From January to April b) From July to October.

Supplementary Table 1. **Amount of methane estimated from bubbles catcher or echosounder surveys compared to this study.** Only current estimations are indicated here, i.e. we do not compare our data with future scenarios. Refer to S.I.5 for distinction between studies.

Supplementary Table 2. **CTD data along the MASOX site.** Parameters are indicated in the first line.

Suppl. Fig. 1

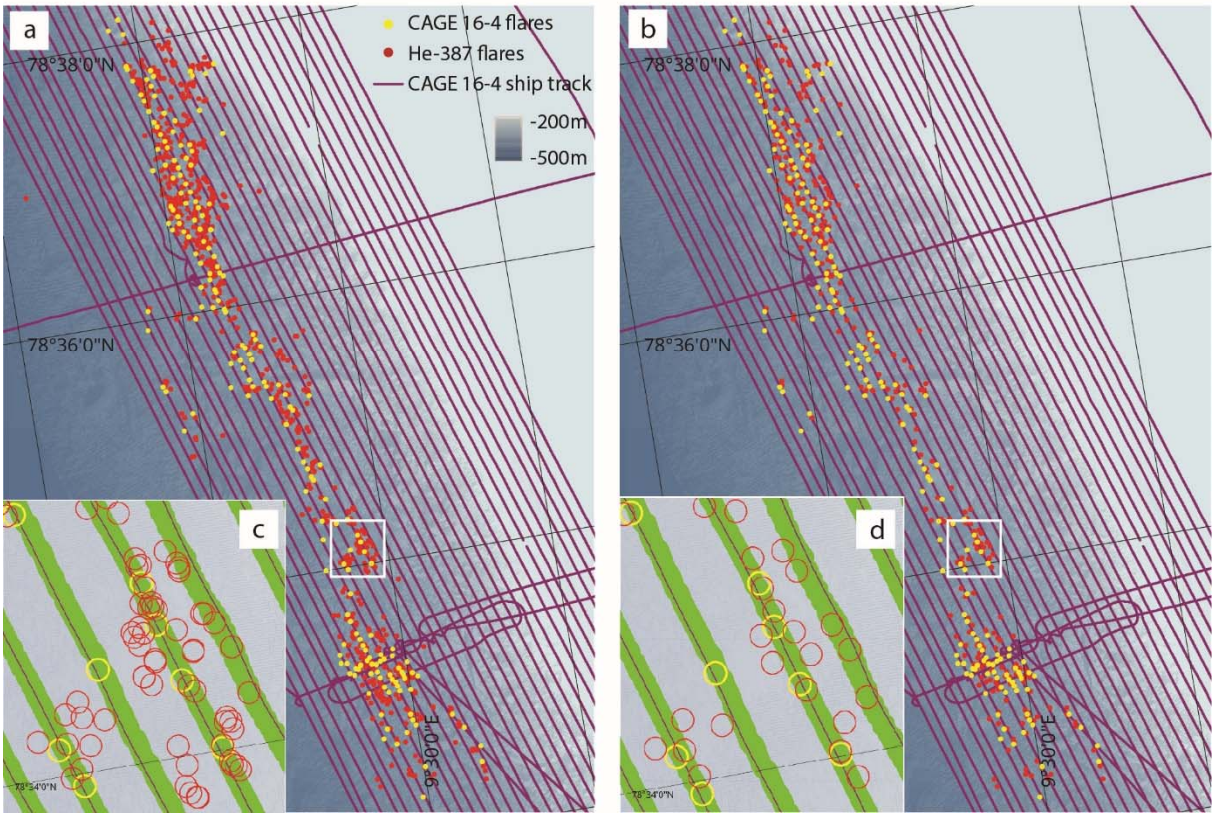

606

607

Suppl. Fig. 2

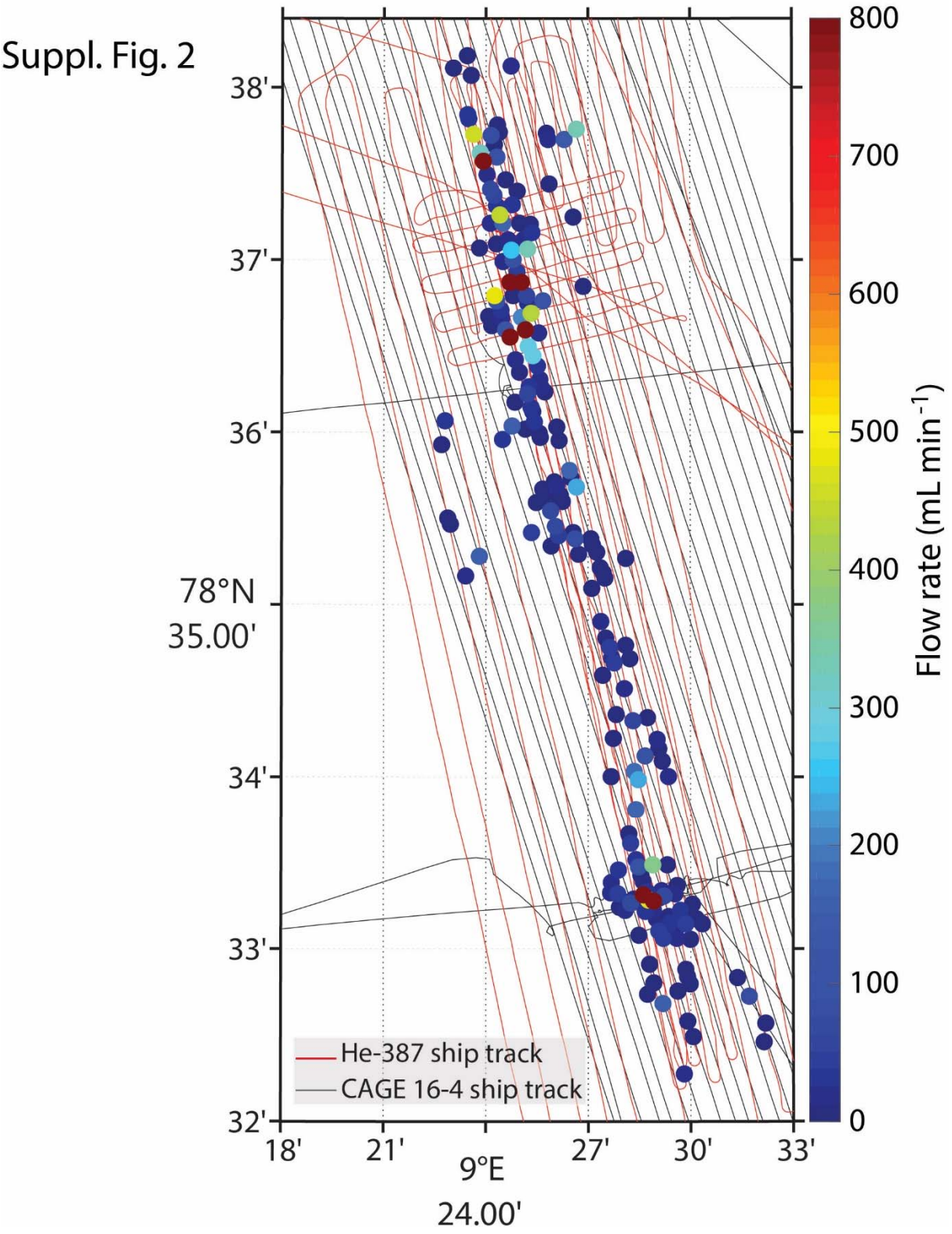

608

609

Suppl. Fig. 3

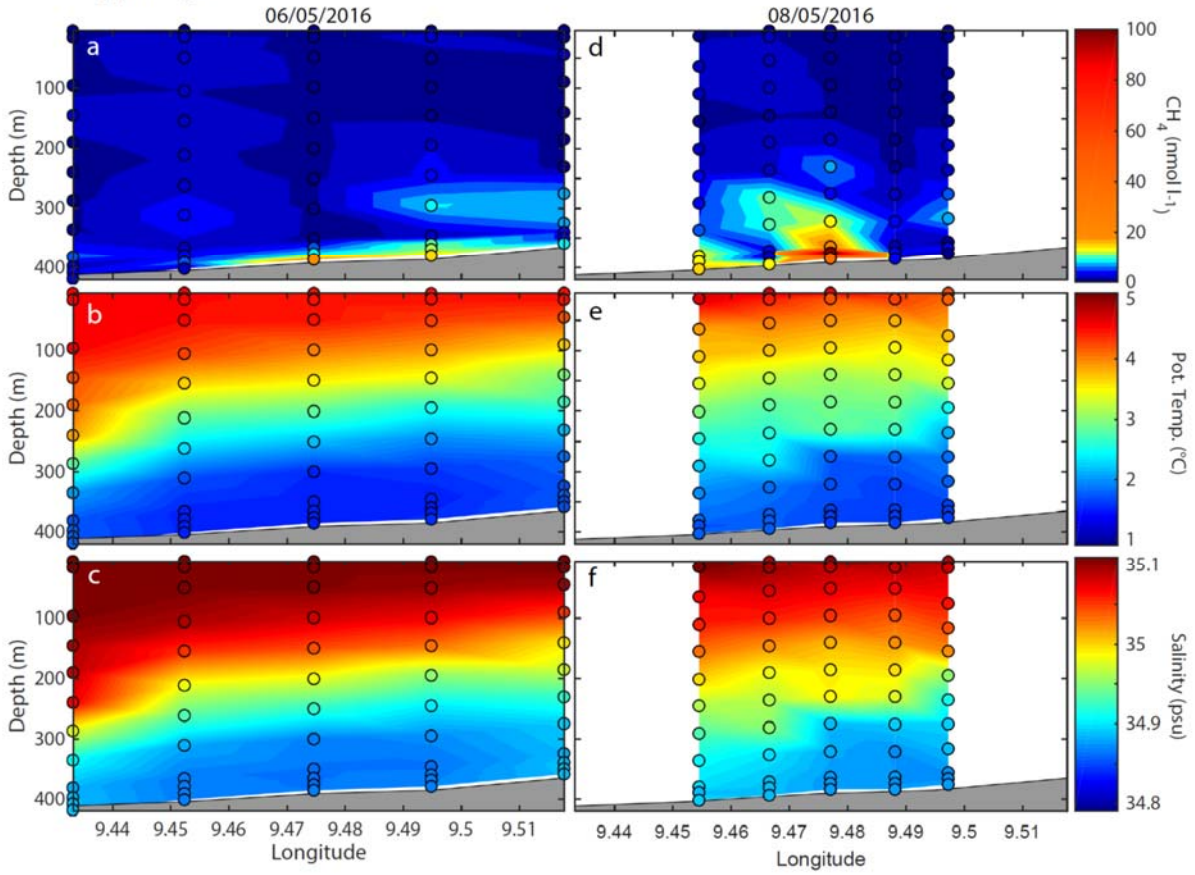

610

611

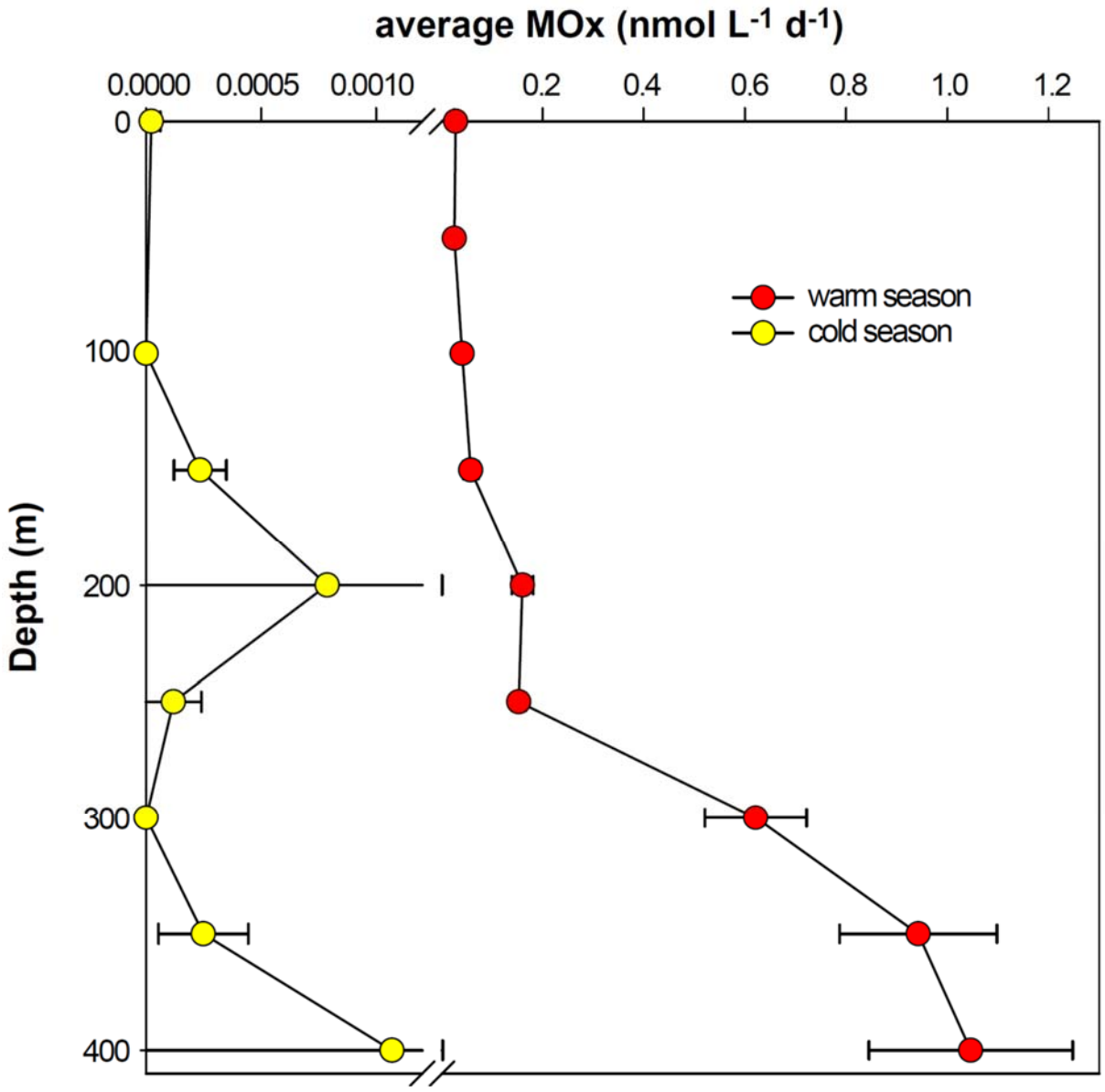
average MOx (nmol L-1 d-1)
0.0000
0.0005
0.0010
0.2
0.4
0.6
0.8
1.0
1.2
0
100
200
300
400
Depth (m)
warm season
cold season

612

613

Supplementary Table 1

Reference	Method	Average bottom water temperature (°C)	Annual CH_4 flux (10^7 mol yr^{-1})	Corrected annual CH_4 flux (10^7 mol yr^{-1})
This study	Echosounder survey	1.7	2.36	-
Sahling et al.[1]	Bubble catcher	4	4*	3.1*
Veloso et al.[8]	Echosounder survey	3	0.7 – 1.1	0.5 – 0.8
Jansson et al.[9]	Echosounder survey	4.2	0.41	0.3
Veloso et al.[10]	Echosounder survey	3	2.5 – 3.9	1.9 - 3

* The value from Sahling et al. has been calculated using the corrected mass flux of 37.1 mmol min^{-1}.

621 **Supplementary Table 2**

Station	Date	Longitude [°E]	Latitude [°N]	Depth [m]	Temperature [°C]	Salinity [PSU]	CH_4 nmol/l
674	06.05.2016	9,433	78,551	418	1,8	34,89	2
674	06.05.2016	9,433	78,551	407	1,8	34,89	4
674	06.05.2016	9,433	78,551	397	1,8	34,89	2
674	06.05.2016	9,433	78,551	381	1,7	34,88	5
674	06.05.2016	9,433	78,551	335	2,0	34,91	1
674	06.05.2016	9,433	78,551	286	2,8	34,98	1
674	06.05.2016	9,433	78,551	239	3,9	35,07	1
674	06.05.2016	9,433	78,551	190	4,1	35,09	1
674	06.05.2016	9,433	78,551	145	4,2	35,09	3
674	06.05.2016	9,433	78,551	96	4,6	35,11	1
674	06.05.2016	9,433	78,551	16	4,6	35,11	1
674	06.05.2016	9,433	78,551	5	4,6	35,11	1
676	06.05.2016	9,452	78,554	401	1,5	34,87	2
676	06.05.2016	9,452	78,554	390	1,5	34,87	5
676	06.05.2016	9,452	78,554	378	1,5	34,87	4
676	06.05.2016	9,452	78,554	365	1,5	34,87	3
676	06.05.2016	9,452	78,554	310	1,7	34,88	4
676	06.05.2016	9,452	78,554	261	2,3	34,93	3
676	06.05.2016	9,452	78,554	211	2,8	34,98	2
676	06.05.2016	9,452	78,554	154	3,7	35,05	3
676	06.05.2016	9,452	78,554	105	4,2	35,09	2
676	06.05.2016	9,452	78,554	50	4,5	35,11	3
676	06.05.2016	9,452	78,554	15	4,5	35,11	2
676	06.05.2016	9,452	78,554	5	4,5	35,11	1
677	06.05.2016	9,475	78,554	385	1,5	34,87	20
677	06.05.2016	9,475	78,554	376	1,5	34,86	8
677	06.05.2016	9,475	78,554	365	1,5	34,86	5
677	06.05.2016	9,475	78,554	349	1,5	34,86	1
677	06.05.2016	9,475	78,554	300	1,6	34,87	1
677	06.05.2016	9,475	78,554	250	2,2	34,92	1
677	06.05.2016	9,475	78,554	200	2,8	34,98	1
677	06.05.2016	9,475	78,554	149	3,5	35,04	1
677	06.05.2016	9,475	78,554	99	4,0	35,08	1
677	06.05.2016	9,475	78,554	49	4,5	35,11	1
677	06.05.2016	9,475	78,554	15	4,5	35,11	1
677	06.05.2016	9,475	78,554	5	4,5	35,11	1
678	06.05.2016	9,495	78,555	378	1,6	34,87	14
678	06.05.2016	9,495	78,555	368	1,6	34,87	11
678	06.05.2016	9,495	78,555	359	1,5	34,87	11
678	06.05.2016	9,495	78,555	345	1,5	34,86	2
678	06.05.2016	9,495	78,555	294	1,6	34,87	8

678	06.05.2016	9,495	78,555	245	2,0	34,90	4
678	06.05.2016	9,495	78,555	194	2,5	34,95	3
678	06.05.2016	9,495	78,555	145	3,4	35,03	1
678	06.05.2016	9,495	78,555	99	3,9	35,07	1
678	06.05.2016	9,495	78,555	50	4,3	35,10	1
678	06.05.2016	9,495	78,555	14	4,5	35,11	2
678	06.05.2016	9,495	78,555	5	4,5	35,11	1
679	06.05.2016	9,518	78,556	358	1,7	34,89	8
679	06.05.2016	9,518	78,556	349	1,7	34,89	4
679	06.05.2016	9,518	78,556	339	1,8	34,89	4
679	06.05.2016	9,518	78,556	323	1,7	34,88	6
679	06.05.2016	9,518	78,556	274	1,8	34,89	7
679	06.05.2016	9,518	78,556	230	2,2	34,92	1
679	06.05.2016	9,518	78,556	185	2,7	34,97	1
679	06.05.2016	9,518	78,556	140	3,0	34,99	NaN
679	06.05.2016	9,518	78,556	90	3,7	35,05	1
679	06.05.2016	9,518	78,556	44	4,2	35,10	2
679	06.05.2016	9,518	78,556	15	4,5	35,11	1
679	06.05.2016	9,518	78,556	5	4,5	35,11	1
681	08.05.2016	9,454	78,553	401	1,8	34,89	15
681	08.05.2016	9,454	78,553	388	1,7	34,89	13
681	08.05.2016	9,454	78,553	379	1,8	34,90	14
681	08.05.2016	9,454	78,553	335	2,0	34,91	5
681	08.05.2016	9,454	78,553	290	2,2	34,93	4
681	08.05.2016	9,454	78,553	245	2,6	34,96	3
681	08.05.2016	9,454	78,553	201	2,9	35,00	2
681	08.05.2016	9,454	78,553	155	3,4	35,03	1
681	08.05.2016	9,454	78,553	110	3,7	35,06	2
681	08.05.2016	9,454	78,553	65	3,9	35,07	2
681	08.05.2016	9,454	78,553	14	4,7	35,11	2
681	08.05.2016	9,454	78,553	4	4,7	35,11	1
682	08.05.2016	9,467	78,554	393	1,8	34,89	13
682	08.05.2016	9,467	78,554	380	1,8	34,89	2
682	08.05.2016	9,467	78,554	371	1,8	34,89	4
682	08.05.2016	9,467	78,554	326	1,9	34,90	9
682	08.05.2016	9,467	78,554	281	2,4	34,95	11
682	08.05.2016	9,467	78,554	236	2,6	34,96	3
682	08.05.2016	9,467	78,554	190	2,8	34,98	2
682	08.05.2016	9,467	78,554	146	3,2	35,02	2
682	08.05.2016	9,467	78,554	100	3,7	35,06	3
682	08.05.2016	9,467	78,554	55	4,0	35,08	2
682	08.05.2016	9,467	78,554	15	4,4	35,10	2
682	08.05.2016	9,467	78,554	5	4,6	35,09	1
683	08.05.2016	9,477	78,556	383	1,7	34,88	41
683	08.05.2016	9,477	78,556	373	1,7	34,88	111

683	08.05.2016	9,477	78,556	363	1,7	34,88	19
683	08.05.2016	9,477	78,556	320	1,7	34,88	13
683	08.05.2016	9,477	78,556	274	1,8	34,89	4
683	08.05.2016	9,477	78,556	229	2,8	34,99	7
683	08.05.2016	9,477	78,556	185	2,9	34,99	2
683	08.05.2016	9,477	78,556	140	3,1	35,01	1
683	08.05.2016	9,477	78,556	95	3,6	35,05	1
683	08.05.2016	9,477	78,556	50	3,9	35,07	1
683	08.05.2016	9,477	78,556	14	4,2	35,09	1
683	08.05.2016	9,477	78,556	5	4,5	35,10	1
684	08.05.2016	9,488	78,556	383	1,7	34,88	3
684	08.05.2016	9,488	78,556	373	1,7	34,87	4
684	08.05.2016	9,488	78,556	363	1,7	34,88	2
684	08.05.2016	9,488	78,556	321	1,6	34,87	4
684	08.05.2016	9,488	78,556	275	1,8	34,89	2
684	08.05.2016	9,488	78,556	230	2,7	34,98	1
684	08.05.2016	9,488	78,556	185	2,9	35,00	1
684	08.05.2016	9,488	78,556	140	3,2	35,02	1
684	08.05.2016	9,488	78,556	95	3,5	35,04	1
684	08.05.2016	9,488	78,556	51	3,8	35,07	1
684	08.05.2016	9,488	78,556	15	4,3	35,09	1
684	08.05.2016	9,488	78,556	4	4,3	35,09	1
685	08.05.2016	9,497	78,557	375	1,7	34,88	1
685	08.05.2016	9,497	78,557	365	1,7	34,87	4
685	08.05.2016	9,497	78,557	355	1,7	34,87	1
685	08.05.2016	9,497	78,557	316	1,8	34,89	8
685	08.05.2016	9,497	78,557	275	1,9	34,89	5
685	08.05.2016	9,497	78,557	235	2,1	34,91	2
685	08.05.2016	9,497	78,557	195	2,5	34,95	2
685	08.05.2016	9,497	78,557	154	3,3	35,02	1
685	08.05.2016	9,497	78,557	116	3,6	35,04	1
685	08.05.2016	9,497	78,557	76	3,7	35,06	1
685	08.05.2016	9,497	78,557	15	4,1	35,08	1
685	08.05.2016	9,497	78,557	5	4,2	35,09	1